JCI The Journal of Clinical Investigation

Retinal angiogenesis suppression through small molecule activation of p53

Sai H. Chavala, Younghee Kim, Laura Tudisco, Valeria Cicatiello, Till Milde, Nagaraj Kerur, Nidia Claros, Susan Yanni, Victor H. Guaiquil, William W. Hauswirth, John S. Penn, Shahin Rafii, Sandro De Falco, Thomas C. Lee, Jayakrishna Ambati

J Clin Invest. 2013;123(10):4170-4181. https://doi.org/10.1172/JCI67315.

Research Article **Vascular biology**

Neovascular age-related macular degeneration is a leading cause of irreversible vision loss in the Western world. Cytokine-targeted therapies (such as anti-vascular endothelial growth factor) are effective in treating pathologic ocular angiogenesis, but have not led to a durable effect and often require indefinite treatment. Here, we show that Nutlin-3, a small molecule antagonist of the E3 ubiquitin protein ligase MDM2, inhibited angiogenesis in several model systems. We found that a functional p53 pathway was essential for Nutlin-3–mediated retinal antiangiogenesis and disruption of the p53 transcriptional network abolished the antiangiogenic activity of Nutlin-3. Nutlin-3 did not inhibit established, mature blood vessels in the adult mouse retina, suggesting that only proliferating retinal vessels are sensitive to Nutlin-3. Furthermore, Nutlin-3 inhibited angiogenesis in nonretinal models such as the hind limb ischemia model. Our work demonstrates that Nutlin-3 functions through an antiproliferative pathway with conceivable advantages over existing cytokine-targeted antiangiogenesis therapies.

Retinal angiogenesis suppression through small molecule activation of p53

Sai H. Chavala,[1] Younghee Kim,[2] Laura Tudisco,[3] Valeria Cicatiello,[3] Till Milde,[4,5] Nagaraj Kerur,[2] Nidia Claros,[4] Susan Yanni,[6] Victor H. Guaiquil,[7] William W. Hauswirth,[8] John S. Penn,[6] Shahin Rafii,[4] Sandro De Falco,[3] Thomas C. Lee,[9] and Jayakrishna Ambati[2]

[1]Department of Ophthalmology, University of North Carolina–Chapel Hill, Chapel Hill, North Carolina, USA. [2]Department of Ophthalmology and Visual Sciences, University of Kentucky College of Medicine, Lexington, Kentucky, USA. [3]Angiogenesis Lab, Institute of Genetics and Biophysics – CNR, Napoli, Italy. [4]Howard Hughes Medical Institute, Ansary Center for Stem Cell Therapeutics, Department of Genetic Medicine, Weill Medical College of Cornell University, New York, New York, USA. [5]Clinical Cooperation Unit Pediatric Oncology, German Cancer Research Center, Heidelberg, Germany. [6]Vanderbilt Eye Institute, Vanderbilt University, Nashville, Tennessee, USA. [7]Laboratory for Soft Tissue Research, Hospital for Special Surgery, New York, New York, USA. [8]Powell Gene Therapy Center, Departments of Ophthalmology and Pediatrics, University of Florida, Gainesville, Florida, USA. [9]Retina Institute, Vision Center, Childrens Hospital Los Angeles, Los Angeles, California, USA.

Neovascular age-related macular degeneration is a leading cause of irreversible vision loss in the Western world. Cytokine-targeted therapies (such as anti-vascular endothelial growth factor) are effective in treating pathologic ocular angiogenesis, but have not led to a durable effect and often require indefinite treatment. Here, we show that Nutlin-3, a small molecule antagonist of the E3 ubiquitin protein ligase MDM2, inhibited angiogenesis in several model systems. We found that a functional p53 pathway was essential for Nutlin-3–mediated retinal antiangiogenesis and disruption of the p53 transcriptional network abolished the antiangiogenic activity of Nutlin-3. Nutlin-3 did not inhibit established, mature blood vessels in the adult mouse retina, suggesting that only proliferating retinal vessels are sensitive to Nutlin-3. Furthermore, Nutlin-3 inhibited angiogenesis in nonretinal models such as the hind limb ischemia model. Our work demonstrates that Nutlin-3 functions through an antiproliferative pathway with conceivable advantages over existing cytokine-targeted antiangiogenesis therapies.

Introduction

Neovascular age-related macular degeneration (NV-ARMD) leads to irreversible vision loss as a consequence of pathologic angiogenesis. Intravitreal use of neutralizing antibodies to VEGF-A provides significant visual rehabilitation (1), but recalcitrant cases are emerging, with one study reporting 45% of NV-ARMD patients not having the desired response to anti-VEGF monotherapy (2). Also, the need for frequent, repeat treatments have clinicians and scientists searching for durable treatments that can reduce dependence on anti-VEGF.

Epimacular and extraocular brachytherapy are cytokine-independent therapies that are currently being evaluated in clinical trial for NV-ARMD (3–5). Ionizing radiation induces free radicals and DNA damage to the cellular genome, ultimately leading to mobilization of the tumor suppression transcription factor p53 (6). The short-term side effect profile appears to be favorable in these clinical trials, but long-term toxicity concerns remain.

Small-molecule MDM2 inhibitors, such as Nutlin-3, have recently been reported and are classically known to disrupt MDM2-p53 interaction leading to p53 activation (7). In vitro and Matrigel plug endothelial cell studies suggest that Nutlin-3 may inhibit angiogenesis (8), but it remains unclear whether Nutlin-3 possesses antiangiogenesis activity that is biologically relevant. Recently, 2 alternative mechanisms that may explain the antiangiogenic activity of Nutlin-3 have been proposed: (a) MDM2 binds to HIF-1α in the p53 binding domain, rendering HIF-1α inactive; (b) stimulation of factor inhibiting HIF (9–13). Both mechanisms ultimately lead to diminished VEGF transcription and are plausible explanations of MDM2-mediated antiangiogenesis. We aimed to determine whether Nutlin-3 has an antiangiogenesis in vivo effect and identify the essential mechanisms involved in Nutlin-3 antiangiogenesis.

Results

To determine whether Nutlin-3 inhibits angiogenesis, we first tested to determine whether Nutlin-3 inhibits proliferation of 2 blood vessel components: endothelial and SMC proliferation. Nutlin-3 is available in racemic form and purified enantiomers Nutlin-3A (active form) and Nutlin-3B (150× less potent than Nutlin-3A). Nutlin-3 inhibited human and rat retinal microvascular endothelial cell (HRMEC and RRMEC), human umbilical vein endothelial cell (HUVEC), and human umbilical vein SMC (HUVSMC) proliferation (Figures 1 and 2, and Supplemental Figures 1 and 2; supplemental material available online with this article; doi:10.1172/JCI67315DS1). HUVECs and HUVSMCs both demonstrated time- and dose-dependent inhibition of cell proliferation, while HUVSMCs were sensitive at higher doses of Nutlin-3 compared with HUVECs (Figures 1 and 2).

Next, we aimed to identify the mechanism that mediates Nutlin-3 HUVEC and HUVSMC inhibition. Immunofluorescence and Western blot studies confirmed Nutlin-3A induces p53 and downstream target p21 in HUVECs and HUVSMCs (Figure 3). We

Conflict of interest: Sai H. Chavala and Thomas C. Lee filed patent application no. 61/386,808, "MDM2 inhibitors for treatment of ocular conditions," on September 27, 2010. Sai H. Chavala is founder of Serrata LLC, a start-up company that plans to commercialize novel treatments for ocular disease.

Note regarding evaluation of this manuscript: Manuscripts authored by scientists associated with Duke University, The University of North Carolina at Chapel Hill, Duke-NUS, and the Sanford-Burnham Medical Research Institute are handled not by members of the editorial board but rather by the science editors, who consult with selected external editors and reviewers.

Citation for this article: *J Clin Invest.* 2013;123(10):4170–4181. doi:10.1172/JCI67315.

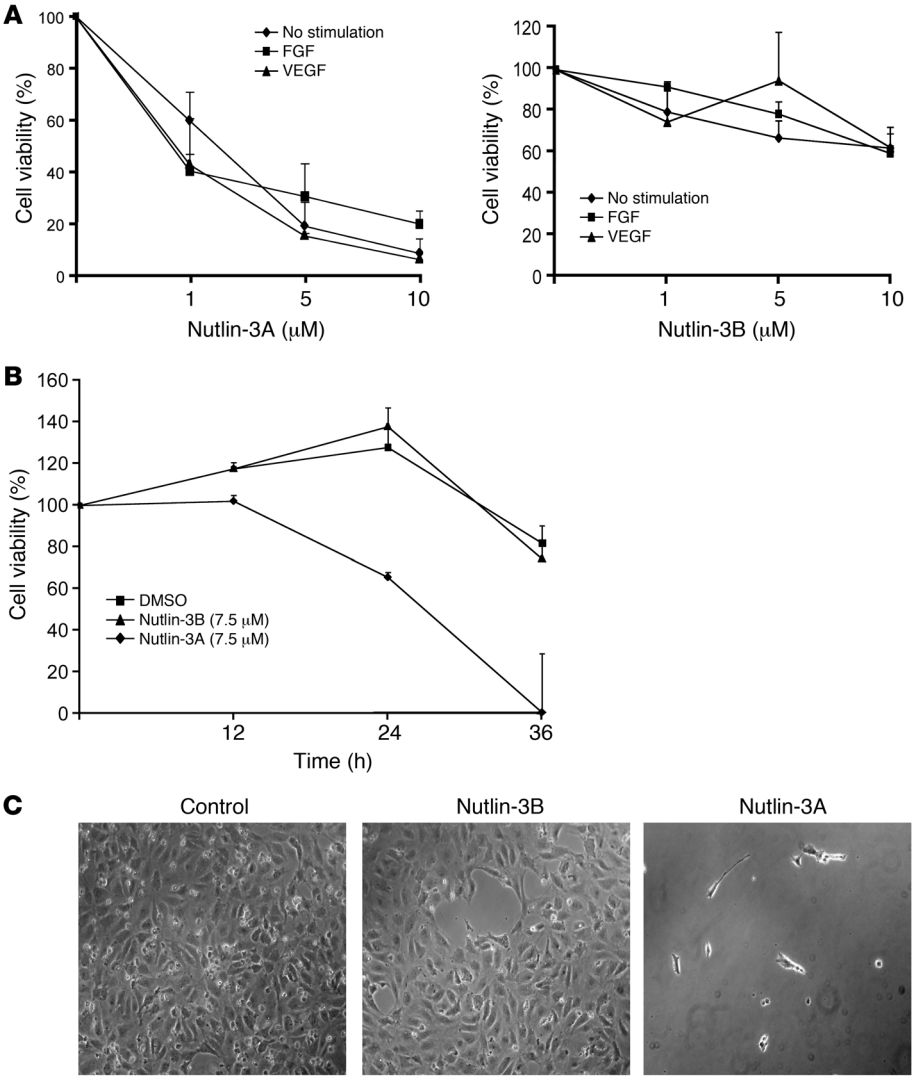

Figure 1
Nutlin-3 inhibits HUVEC proliferation. (**A**) Nutlin-3A or Nutlin-3B in 1, 5, or 10 μM concentrations was added to proliferating HUVECs for 36 hours. HUVECs were either unchallenged or challenged with VEGF-A or FGF-2 during the incubation. (**B**) Cell viability was measured at 12, 24, and 36 hours after incubation. (**C**) Phase contrast images of representative conditions of serum free, unchallenged HUVECs at 36 hours. Original magnification, ×100.

predicted activation of p53 and subsequent downstream targets may inhibit cell proliferation by initiating the apoptosis pathway. After 24 hours of incubation with Nutlin-3, flow cytometry demonstrated significantly more double-positive annexin V and propidium iodide HUVECs compared with control cells (Figure 4A). Quantitative RT-PCR (qRT-PCR) demonstrated a relative increase in the ratio of *BAX* to *BCL-2* (Figure 4D), and increased TUNEL-positive cells in Nutlin-3–treated HUVECs in serum-depleted medium with growth factor supplementation undergo apoptosis, contrary to a previous report that Nutlin-3 alone is insufficient to mediate HUVEC apoptosis (Figure 4, B and C, and ref. 8). Similar experiments demonstrate that Nutlin-3 does not cause HUVEC apoptosis in growth medium (Supplemental Figure 3), but does cause HRMEC apoptosis in growth medium (Supplemental Figure 1, B and C). Surprisingly, HUVSMCs treated for 36 hours with Nutlin-3 did not undergo apoptosis despite upregulation of p53 within 8 hours (Figure 3D and Figure 4, E and F).

To determine the necessity of the p53 pathway for the observed Nutlin-3–mediated cellular effects, we infected HUVECs with retrovirus expressing either control shRNA or p53 shRNA. Cell viability assay demonstrated that p53 shRNA–infected cells had become resistant to Nutlin-3A inhibition (Figure 5). Similar cell viability experiments using RRMECs and 2 different siRNA p53 sequences revealed minimal Nutlin-3 activity (Supplemental Figure 2). These data suggest that the p53 pathway is critical for Nutlin-3–mediated inhibition of endothelial cells.

To test the hypothesis that Nutlin-3–mediated cell death inhibits angiogenesis, we performed a capillary tube formation assay that measures the ability to form tube-like structures. Our experiments revealed a 93% reduction in capillary tube formation in Nutlin-3A–treated HUVECs compared with control. Also, the effects of Nutlin-3A on inhibiting capillary tube formation appeared to be dose dependent (Figure 6).

Next, we used a retinal development model to test the possibility that Nutlin-3 could be used to inhibit retinal vessel proliferation (Figure 7) (14). We found that subcutaneous Nutlin-3 injection in the nape revealed a modest (27.4%), but statistically significant, reduction ($P < 0.05$) in the amount of retinal vessels compared with those in sham-injected mice (Figure 7, B and C). In an attempt to reduce systemic toxicity and improve delivery to the eye, we performed similar experiments and injected Nutlin-3 in the periorbital area under the fused eyelid (15). In these experiments, we found 43.8% fewer blood vessels compared with those in the sham-injected mice ($P < 0.01$) (Figure 7, D and E). Although a rare

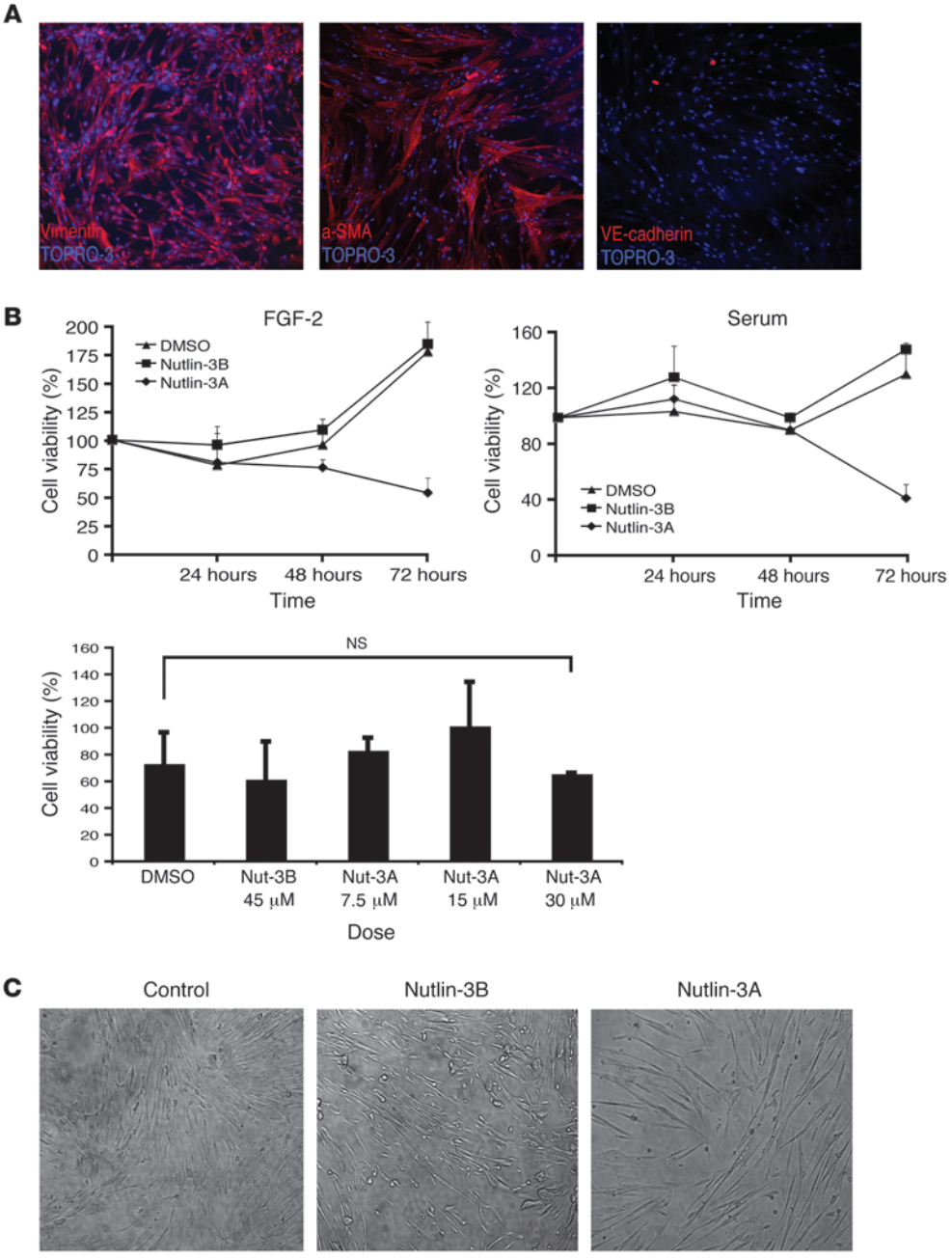

Figure 2
Nutlin-3 inhibits HUVSMC proliferation. (**A**) Confocal immunofluorescence images are displayed characterizing HUVSMCs. The panels indicate that these cells are vimentin (left panel) and smooth muscle actin (middle panel) positive but VE-cadherin (right panel) negative. Original magnification, ×200. (**B**) Vehicle, Nutlin-3B (Nut-3B) (7.5 μM), or Nutlin-3A (7.5 μM) was added to proliferating HUVSMCs at various time points with FGF-2 or 5% FBS. Various concentrations (0, 7.5, 15, 30 μM) of Nutlin-3A were added to cultures of serum-free, unchallenged HUVSMCs for 24 hours (lower panel). (**C**) Representative images of serum-free HUVSMCs supplemented with FGF-2 after 72 hours of culture. Original magnification, ×100. Data are mean ± SD and representative of 4 separate experiments performed in at least duplicate. NS, $P > 0.05$.

event, we were able to detect TUNEL-positive cells that colocalized to the retinal endothelium (*Griffonia simplicifolia*–isolectin B4 [GS-IB4] lectin stained) in a Nutlin-3–treated eye (Figure 7F).

We entertained the possibility that Nutlin-3 may work through noncanonical pathways in vivo. Laser-induced choroidal neovascularization (CNV) is an established model of pathologic ocular angiogenesis (16). Hif-1α and VEGF protein expression are significantly increased in CNV lesions, and it is conceivable that Nutlin-3–mediated antiangiogenesis also occurs through Hif-1α (17). We performed a single intravitreal injection of racemic Nutlin-3 or DMSO immediately after laser injury and demonstrated that, after 7 days, Nutlin-3 inhibits pathologic retinal angiogenesis in a dose-dependent fashion, with peak effect at 10 ng/μl (17.2 μM) (Figure 8, A and B). To decipher the critical pathway responsible for Nutlin-3–mediated antiangiogenesis, we performed similar laser-induced CNV experiments in $p53^{-/-}$ mice and conditionally inactivated HIF-1α and VEGF-A mice. We observed no statistically significant difference in Nutlin-3–treated mice in $p53^{-/-}$, $Hif1a^{flox/flox}$, and $Vegfa^{flox/flox}$ mice compared with controls (Figure 8, C and D, and Supplemental Figure 4).

Thus far, we examined the effect of Nutlin-3A on proliferating cells in vitro and in vivo. To determine whether Nutlin-3 has an effect on established, nonproliferating blood vessels, we injected Nutlin-3 in the vitreous cavity of adult mice. Our analysis demonstrated that there was no reduction of the retinal vasculature in the Nutlin-3–treated eyes compared with the control ($P > 0.05$) (Figure 9). Additionally, we were interested in examining the potential side effect of neuronal degeneration caused by Nutlin-3. On H&E

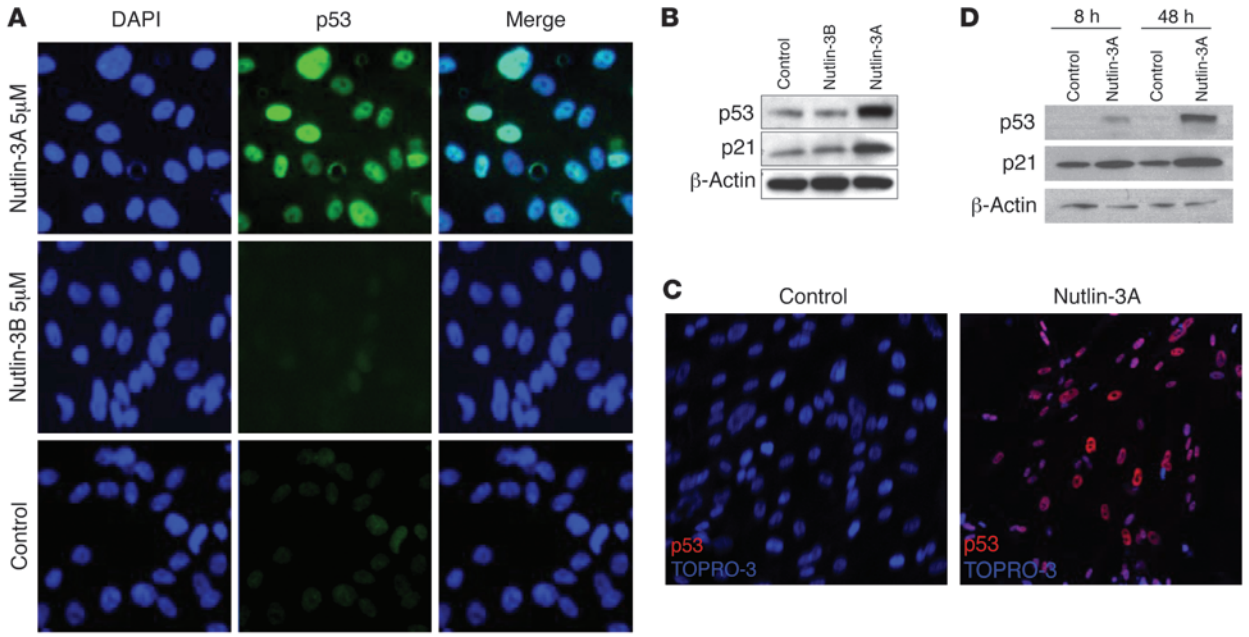

Figure 3

Nutlin-3 induces p53 expression and a downstream target in HUVECs and HUVSMCs. (**A**) HUVECs were seeded on plastic-bottom culture dishes precoated with gelatin and treated with either 5 μM of Nutlin-3A, 5 μM of Nutlin-3B, or vehicle after 8 hours. Images were taken with an epifluorescent microscope and are representative of p53 expression (middle column) in the nucleus (left column) of HUVECs. Original magnification, ×400. (**B**) Western blot analysis for p53 and p21 was performed on lysates obtained from HUVECs treated with Nutlin-3A, Nutlin-3B, or vehicle in various concentrations for 8 hours. (**C**) Representative magnified confocal images are shown of HUVSMCs treated with either 7.5 μM of Nutlin-3A or vehicle after 8 hours. Original magnification, ×200. Nuclear p53 expression is shown in red and TO-PRO-3, a nuclear stain, in blue. (**D**) Western blot analysis for p53 and p21 was performed on lysates obtained from HUVSMCs treated with Nutlin-3A or vehicle.

staining, we did not observe any gross changes in the thickness of the neuronal cell layers of the Nutlin-3–treated eyes (Figure 9B). These data suggest that Nutlin-3 does not cause vascular obliteration of existing retinal vessels or is grossly toxic to the neurosensory retina. It also suggests that, like radiation, MDM2 inhibitors preferentially target proliferating cells more than nonproliferating mature retinal vessels (3, 18).

To determine whether Nutlin-3 inhibits nonocular angiogenesis, we performed experiments using the hind limb ischemia model. After femoral artery ligation, three different concentrations of Nutlin-3 or vehicle control were administered intramuscularly at the time of surgery and 2 days thereafter. At day 7, muscles from ischemic and contralateral hind limb were harvested and processed to quantify blood and lymphatic vessels with CD31/LYVE-1 immunohistochemistry. The extent of vascularization was reported as ischemic to nonischemic ratio, after normalization on myocyte number (Figure 10). The delivery of Nutlin-3 at 86 μM induced a significant inhibition on new blood vessel formation (–40.15%, $P = 0.0316$) without affecting lymphangiogenesis (Supplemental Figure 5).

Discussion

Nutlin-3 is well known to inhibit tumor cell proliferation and angiogenesis, but the precise mechanism of how Nutlin-3 inhibits angiogenesis is unclear. The 2 prevailing hypotheses are that Nutlin-3 inhibits angiogenesis by reducing tumor load and subsequently stimulus for angiogenesis and that Nutlin-3 induces p53-mediated endothelial cell death. A physiologic nontumor angiogenesis model is required to decipher the mechanism, so we chose retinal angiogenesis models.

We chose a murine retinal vascular development model to investigate the role of Nutlin-3 as a solitary agent for inhibiting in vivo angiogenesis. Normal murine retinal vascular development begins in utero and continues after birth (Figure 7A). This model is advantageous for the following reasons: (a) the system does not rely on a tumor model, so we could study the direct effect of MDM2 inhibition on blood vessels, and (b) this in vivo model does not require injury or the addition of supraphysiological doses of proangiogenic cytokines. Our in vivo data demonstrate that Nutlin-3 is capable of inhibiting retinal vascular development. We were able to show this using 2 slightly different models of drug delivery. In our systemic subcutaneous injection experiments, we demonstrated a modest, but statistically significant ($P < 0.05$), inhibition of the retinal vasculature between Nutlin-3–treated mice and sham-injected mice. This difference was accentuated when we delivered periocular injections, presumably due to higher concentrations of the drug at the local site. Periocular drug delivery was chosen because it is an established route of administration commonly used in clinical practice (19). In addition, this method of drug delivery does not cause retinal trauma, an important factor for quantitative analysis in neonatal mouse pups with small retinas. Also of note, experiments evaluating either route of drug delivery were preformed with controls within the same litter. Several independent experiments were performed, and the largest litters were represented. We discovered variations in retinal vascular growth between litters of the same aged mice precluding analysis

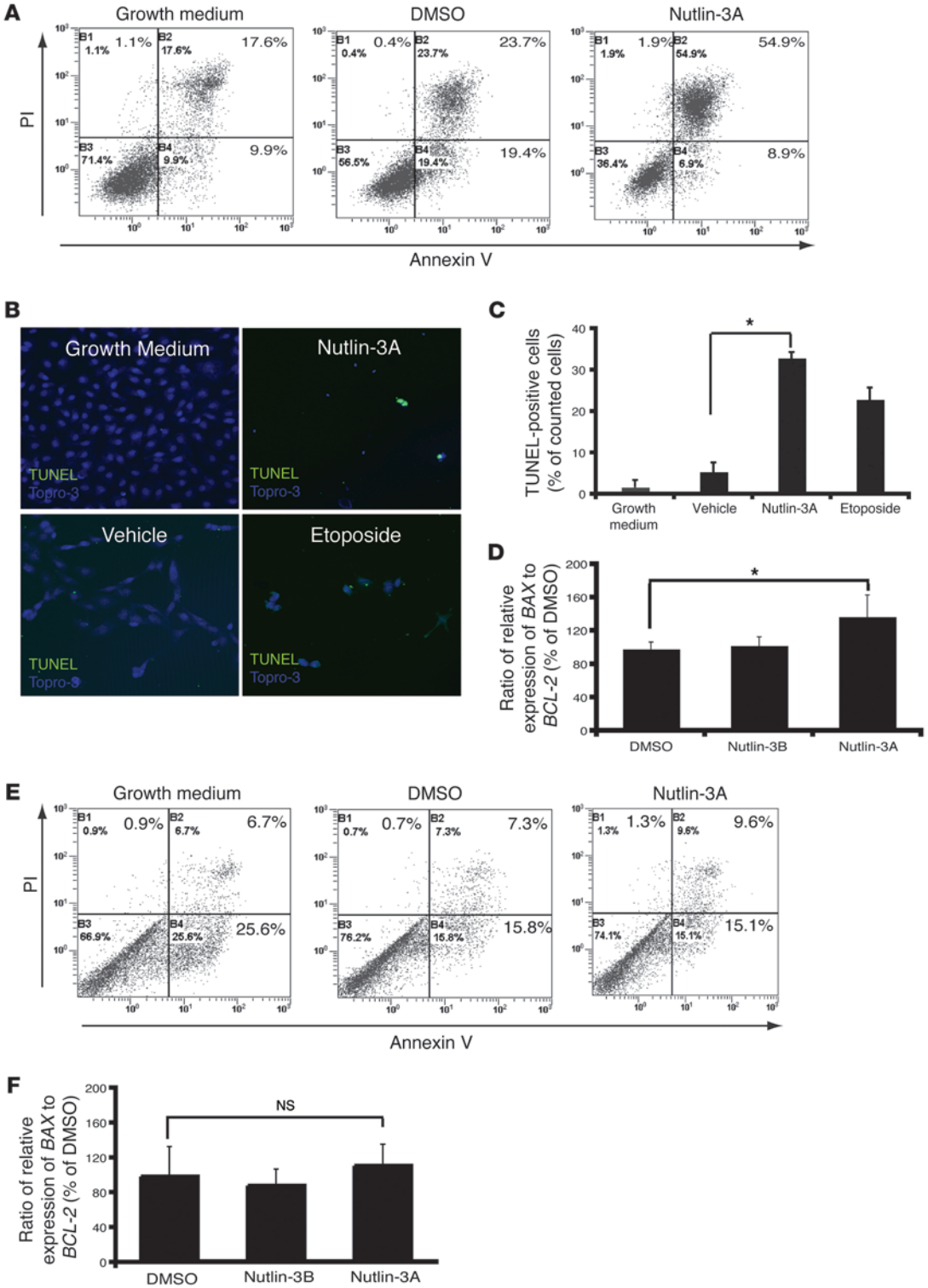

Figure 4

Nutlin-3 induces apoptosis in HUVECs but not in HUVSMCs. (**A**) Representative HUVEC flow cytometry plots from 3 independent experiments were run in duplicate for 8 hours. (**B**) TUNEL staining images of HUVECs. Original magnification, ×200. (**C**) The ratio of the number of TUNEL-positive cells to the number of nuclei found in 5 random fields from each condition are counted by 2 masked observers. Data are mean ± SD and represent 2 independent experiments. (**D**) qRT-PCR of HUVECs treated for 4 hours. Relative *BAX* and *BCL-2* expression are presented as a ratio. Values are provided as a percentage of DMSO (control) and expressed as mean ± SD. (n = 9 from 3 independent experiments).*$P < 0.05$. (**E**) Representative HUVEC flow cytometry plots from 3 independent experiments were run in duplicate for 36 hours. (**F**) qRT-PCR of *BAX* and *BCL-2* expression in HUVSMCs treated for 4 hours. Values are provided given as a percentage of DMSO (control) ± SD. (n = 12 from 4 independent experiments) NS, $P > 0.05$. Amount of Nutlin-3A and Nutlin-3B was 7.5 μM and that of Etoposide was 10 μM.

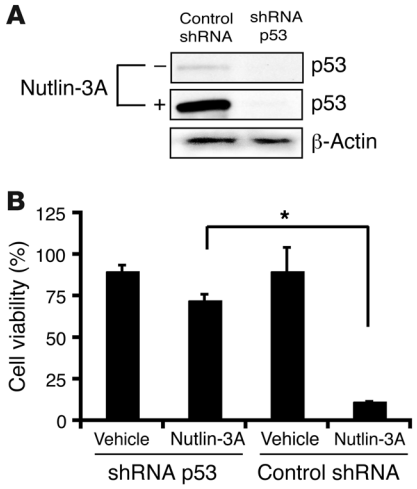

Figure 5
p53 is necessary for Nutlin-3–mediated cell death. (**A** and **B**) HUVECs were infected with a lentiviral vector expressing p53 or control shRNA for 48 hours and then underwent puromycin selection for 72 hours. (**A**) Cell lysates for Western blot analysis were used to confirm knockdown of p53 in shRNA-infected HUVECs. (**B**) p53 shRNA– and control shRNA–infected HUVECs were seeded at 1×10^6 cells in 6-well plates and incubated with FGF-2 and either Nutlin-3A (7.5 μM) or vehicle (DMSO) for 48 hours. Cell proliferation was measured at 48 hours by manual counting using trypan blue exclusion. Data represent mean ± SD. *$P < 0.05$.

of all the mice as one group. This may be due to differences in litter size, where larger litters produced on average smaller pups and smaller litters produced relatively larger pups. We hypothesize that, like humans, smaller pups have differences in retinal vascular maturation compared with larger pups of the same age. Therefore, only intralitter analysis was performed.

In addition to Nutlin-3's effect on endothelial cells, our study is the first, to our knowledge, to show it inhibits the in vitro proliferation of SMCs (Figure 2). We discovered that HUVSMCs initiate a rapid p53 response to Nutlin-3 similar to HUVECs, but HUVSMCs may not be as sensitive to p53 upregulation witnessed by a delay in cell death. Interestingly, we did not find that Nutlin-3–treated HUVSMCs undergo apoptosis as HUVECs do. In our mouse retina model, we found that first- and second-order vessels can have SMCs around blood vessels, suggested by smooth muscle actin whole-mount antibody staining (Supplemental Figure 6). In our analysis, we observed that Nutlin-3 preferentially targeted capillaries and smaller blood vessels (data not shown). This suggests the possibility that blood vessels ensheathed by SMCs may be protected from Nutlin-3, although this could not be confirmed with in vitro experiments (data not shown).

Laser-induced injury is considered a classic model of CNV (20). We demonstrated that Nutlin-3 inhibits CNV in a dose-dependent manner and that functional p53 is essential for Nutlin-3–mediated antiangiogenesis using p53-knockout mice. Since Nutlin-3 has been reported to inhibit HIF-1α expression (9, 11), we conditionally inactivated HIF-1α in retinal pigment epithelium (RPE) (AAV1-*VMD2*-Cre) using a Cre-loxP system, to evaluate the importance of the HIF-1α pathway for Nutlin-3 function. HIF-1α inactivation alone substantially reduced CNV volume in the laser injury model as expected, but had no further impact on Nutlin-3 antiangiogenesis (Figure 8D). To test the downstream target of HIF-1α, similar laser-induced CNV experiments in $Vegfa^{loxp/loxp}$ were performed and correlated with HIF-1α data, demonstrating no further Nutlin-3 antiangiogenesis with VEGF-A inactivation (Supplemental Figure 4).

Interplay between the HIF-1α and p53 pathways has been well documented, and interestingly, both a synergistic and an antagonistic affect have been reported (10). RPE-derived HIF-1α is known to be an important factor for laser-induced CNV (21). Oxygen availability is a key regulator and determinant of HIF-1α and p53 expression (10). These interactions deserve further study in the laser CNV model, and relative oxygen status, mediated through HIF-1α, may lead to differential Nutlin-3 activity.

In summary, we demonstrate that Nutlin-3 substantially reduces retinal angiogenesis. We provide evidence that a functional

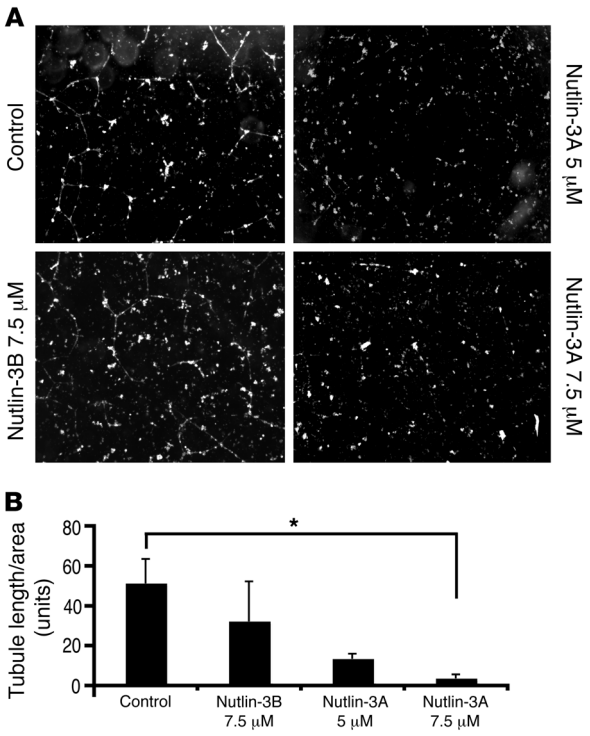

Figure 6
Nutlin-3 inhibits capillary tube formation. (**A**) HUVECs were seeded on Matrigel matrix and incubated with FGF-2 and 7.5 μM of Nutlin-3A, 5 μM of Nutlin-3A, 7.5 μM of Nutlin-3B, or vehicle (DMSO). The images were taken with an inverted light microscope and are representative of capillary tube formation at 24 hours. Original magnification, ×100. (**B**) Quantification of Nutlin-3A–mediated capillary tube formation inhibition. Results are expressed as a ratio of tubule length measured to total area examined ± SEM. *$P < 0.05$.

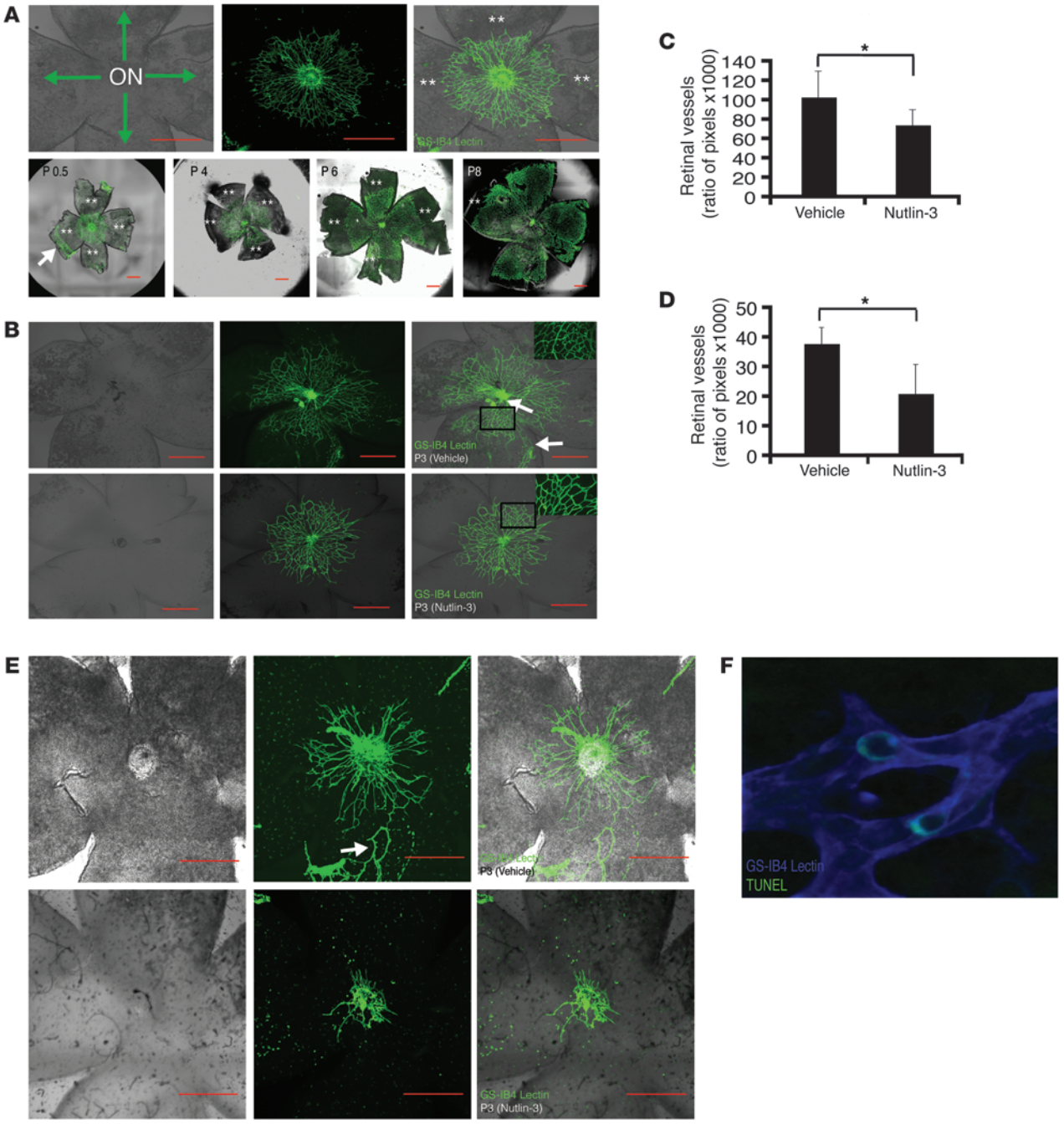

Figure 7

Nutlin-3 inhibits postnatal retinal vascular proliferation. (**A**) Postnatal mouse retinal vascular development after birth (upper left panel). The optic nerve (ON) at the center of a retinal whole mount with green arrows indicating the direction of postnatal blood vessel growth (upper middle and right panels). GS-IB4 lectin staining of a retinal whole mount in the developing mouse pup demonstrating radial growth pattern of postnatal development of retinal vasculature. (lower panels). Double asterisks indicate areas of avascular retina. (**B** and **C**) Neonatal mice were given subcutaneous injections in the nape. (**B**) The retinal vasculature is abrogated in the Nutlin-3–treated eyes ($n = 6$) (bottom row) compared with the sham-injected mice ($n = 4$) (middle row). In addition, we noticed loss of smaller caliber vessels (inset, right column) in the Nutlin-3–treated mice. (**C**) The graph represents retinal vasculature measured as a function of pixels compared with the amount of retinal tissue in each mouse eye (*$P < 0.05$, representative of 2 independent experiments). (**D** and **E**) Neonatal mice were injected in the periocular area of each eye. (**E**) Nutlin-3–treated (lower row) mice ($n = 8$) have less retinal vasculature compared with sham-injected mice ($n = 8$) (upper row). (**D**) Same quantification method used in **B** shows a statistically significant difference between the 2 groups (*$P < 0.01$, representative of 2 independent experiments). (**F**) Rare TUNEL-positive cells identified in the retinal vasculature of a Nutlin-3–treated mouse. Original magnification, ×400. White arrows point to residual fetal vasculature unable to be removed during dissection. Data represent mean ± SD. *$P < 0.05$. Scale bars: 500 μm.

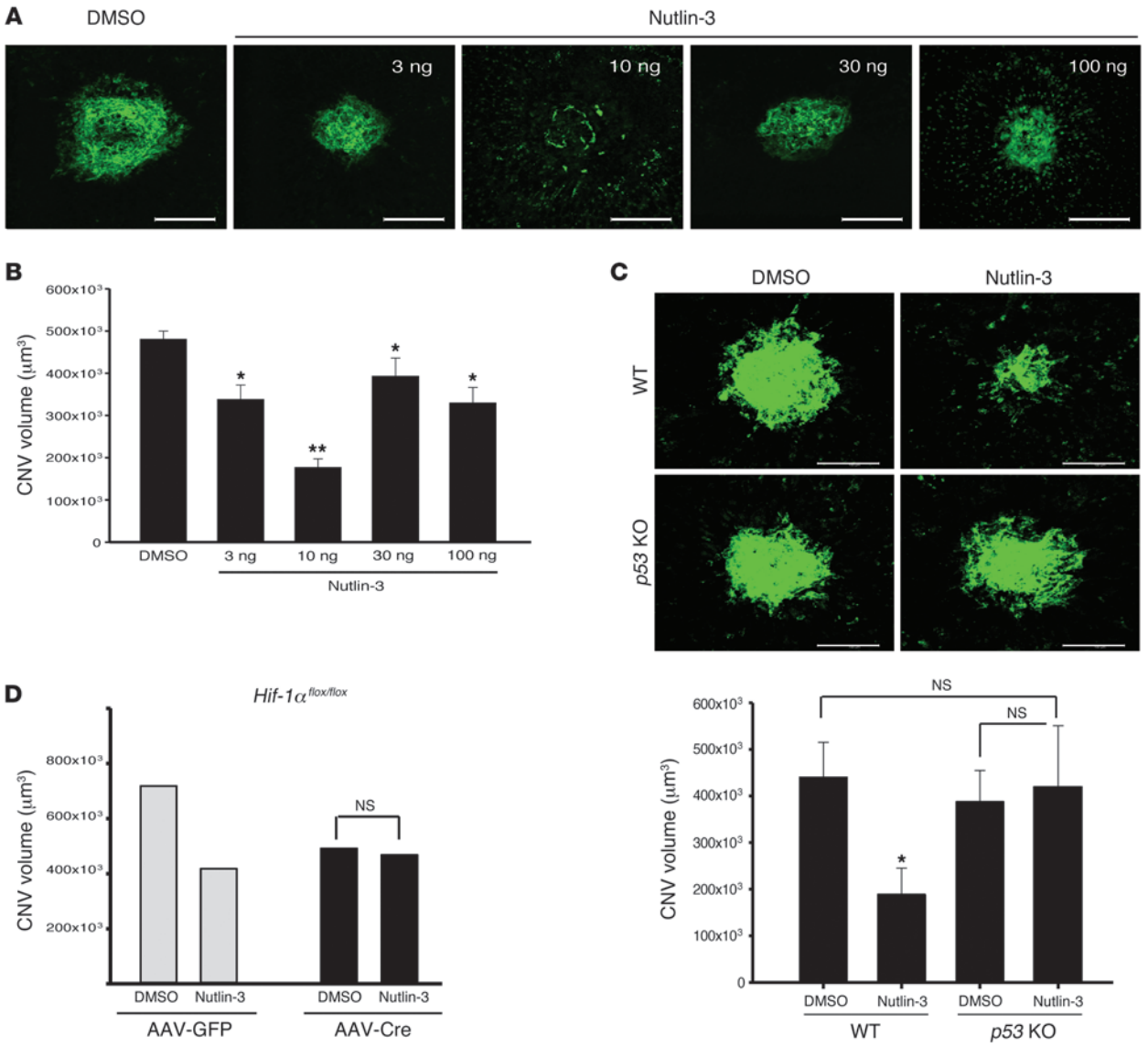

Figure 8

Nutlin-3 inhibits pathologic retinal angiogenesis through the p53 pathway. (**A**) Stacked confocal image of representative laser-induced CNV lesions in racemic Nutlin-3– and DMSO-treated eyes. Racemic Nutlin-3 showed maximal activity at 10 ng/17.2 μM. (**B**) Quantification of *z*-stack confocal images of laser induced CNV in the respective conditions (n = 16–40). (**C**) Representative images of littermate controls (upper panels) after intravitreal injection of DMSO and racemic Nutlin-3. Similar experiments in $p53^{-/-}$ mice demonstrated no appreciable difference between DMSO- and Nutlin-3–injected mice. (n = 10–13). (**D**) $Hif1a^{flox/flox}$ mice were given either subretinal AAV1-*VMD2*-Cre or AAV1-*VMD2*-GFP. HIF-1α inhibition had no additional impact on Nutlin-3 antiangiogenesis (n = 6–10). Data represent mean ± SEM. $^*P < 0.05$; $^{**}P < 0.0001$; NS = $P > 0.05$. $P = 0.052$ for AAV1-GFP-DMSO vs. AAV1-GFP–Nutlin-3. Scale bars: 100 μm.

p53 pathway is critical for Nutlin-3–mediated antiangiogenesis. It is conceivable that these effects are restricted to Nutlin-3 and that other MDM2 inhibitors work differently. Furthermore, we were able to extend our observations to a nonretinal angiogenesis model by demonstrating Nutlin-3 antiangiogenesis in a hind limb ischemia model.

Epimacular and juxtascleral brachytherapy are being evaluated in clinical trials with mixed success (3, 5). MDM2 inhibitors may have a more attractive side effect profile, since they do not elicit DNA damage and, with repeat administration, may even be more robust than a single radiation treatment. Our in vivo results suggest that MDM2 inhibitors, such as Nutlin-3, offer a new therapeutic strategy for inhibiting retinal angiogenesis and may be complementary to existing treatments. Optimization or investigation of other MDM2 inhibitors is attractive for the treatment of NV-ARMD.

Methods

Reagents and antibodies. Nutlin-3A and Nutlin-3B were donated by Lubo Vassilev (Hoffmann-La Roche Inc.) and used for all experiments except for in vivo and RRMEC and HRMEC experiments. Racemic Nutlin-3 (Sigma-Aldrich), which contains a 50:50 mixture of Nutlin-3A and Nutlin-3B and is approximately half as potent as equal concentrations of Nutlin-3A,

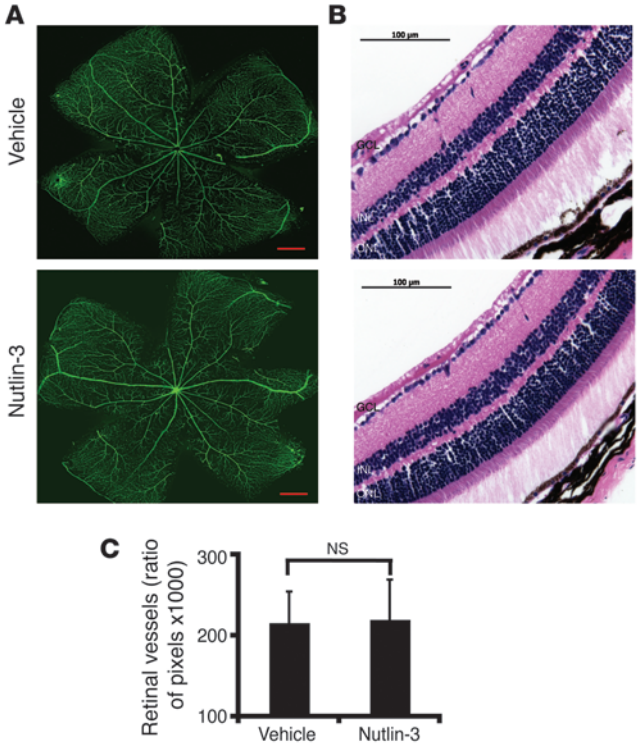

Figure 9
Nutlin-3 does not target preexisting blood vessels. (**A** and **B**) Adult mice received a single intravitreal injection of Nutlin-3 or DMSO to investigate the effects of Nutlin-3 on established blood vessels. (**A**) Confocal images of GS-IB4 lectin–stained and (**B**) H&E-stained paraffin-embedded sections of retinal vasculature 5 days after injection. Scale bars: 500 μm (**A**); 100 μm (**B**).(**C**) Quantification of retinal vessels shows no difference between sham- ($n = 8$) and Nutlin-3–injected mice ($n = 8$) Data represent mean ± SD. NS, $P > 0.05$, summation of 2 independent experiments.

was used for these experiments. For hind limb ischemia experiments, Nutlin-3 (Sigma-Aldrich) was dissolved in 4% ethanol, 35% propylene glycol (Fisher Scientific), 10% PEG-400 (Sigma-Aldrich), and 51% PBS as previously reported at 100 μg/ml (172 μM) (22).

Primary antibodies included the following: mouse p53 antibody (1:100 [Western blot] and 1:50 [Immunofluorescence]; Santa Cruz Biotechnology Inc.), mouse p21 antibody (1:100; Oncogene), rat β-actin (1:1,000; Sigma-Aldrich), mouse smooth muscle actin clone 1A4 (1:100 [whole mount and cells]; Dako), goat VE-Cadherin (1:100; R&D Systems), and mouse vimentin (1:25; Dako). Secondary antibodies included the following: HRP anti-rabbit (1:10,000; Amersham) and HRP anti-mouse (1:10,000; Amersham) for Western blot analysis and Cy2 and Cy3 anti-mouse (Jackson Immunoresearch), used for immunofluorescence. TO-PRO-3 (1:1000; Molecular Probes/Invitrogen) and DAPI (1:1000; Vector Laboratories) were used for nuclear staining. GS-IB4–FITC (1:200; Vector Laboratories) and GS-IB4–Alexa Fluor 644 (20 mg/ml; Molecular Probes) were used for staining the retinal vasculature. Anti-CD31 (BD Biosciences) or anti–LYVE-1 antibodies (Abcam), followed by biotin-labeled goat anti-rat secondary antibodies (Dako), were used to stain blood vessels for hind limb ischemia.

Cell harvest. HUVECs and HUVSMCs (gifts of George Lam and Fan Zhang, Cornell University, New York, New York, USA) were isolated from the umbilical cord veins with collagenase and were cultured in M199 medium containing 10% (vol/vol) FBS, 20 μg/ml endothelial cell growth factor, 50 μg/ml heparin, 100 μg/ml penicillin, and 100 μg/ml streptomycin in a humidified incubator at 37°C with air/5% CO_2. HUVEC and HUVSMC monolayers from passages 2–4 were used in these studies. HRMECs (Cell Systems) were incubated in culture containing endothelial basal medium (EBM) (Cambrex), 10% FBS, and antibiotic/antimycotic solution (Sigma-Aldrich). RRMECs (Cell Biologics Inc.) were cultured following the supplier's instruction.

Cell proliferation assay. Cells were seeded at a concentration of 2×10^5 for HUVECs and 2×10^4 for HUVSMCs in serum-free medium on 12-well plates after detachment. The cells were allowed to adhere overnight in growth medium and then incubated with X-VIVO medium (Cambrex) with or without cytokines (10 ng/ml FGF-2 and 2 μg/ml heparin or 10 ng/ml VEGF-A). For HRMEC experiments, cells were seeded at a concentration of 1×10^5 and allowed to settle overnight in 6-cm plates coated with attachment factor (Cell Signaling). The next day, fresh 10% FBS and EBM medium was added. For HUVEC and HUVSMC cell experiments, an equivalent dilution of 100% DMSO, Nutlin-3A, or Nutlin-3B was added at concentrations indicated in the results the following day. HRMEC experiments were performed in a similar fashion in serum with racemic Nutlin-3 because of the limited availability of Nutlin-3A and Nutlin-3B. Since racemic Nutlin-3 contains a 50:50 mixture of Nutlin-3A and Nutlin-3B, a higher dose of racemic Nutlin was utilized for these experiments compared with those used for HUVECs. After incubation, HUVECs were detached with collagenase/EDTA, and HUVSMCs and HRMECs were detached with trypsin/EDTA. The cells were manually counted with a Hemacytometer (Hausser Scientific) using Trypan blue exclusion.

Matrigel tube assay for in vitro angiogenesis. Matrigel matrix (BD) was kept on ice for 24 hours. Then, 200 μl of Matrigel was added to each well of a 24-well culture plate. After hardening the Matrigel at 37°C for 30 minutes, gels were overlaid with 500 μl of X-VIVO medium containing 3×10^4 HUVECs. Next, endothelial cells were stimulated with 10 ng/ml of FGF-2 and 2 μg/ml heparin and then incubated with various concentrations of DMSO, Nutlin-3A, or Nutlin-3B, in triplicate, as indicated in the results. The effect of Nutlin was inspected 24 hours under an inverted light microscope. Nine overlapping images with a ×10 objective were taken of each well to perform tubule-length quantification. Adobe Photoshop 7.0 (Adobe Systems Inc.) was used to make a montage image of each well. Each montage image was then imported into LSM Image Browser v3.5 (Carl Zeiss Inc.) to measure tubule length. Tubule length was then standardized to the overall pixel area examined. A masked observer assessed all measurements.

Western blot analysis. HUVECs and HUVSMCs were incubated at 2×10^6 in X-VIVO medium and HRMECs in EBM with 10% FBS under various conditions, as reported in the results. Western blot extracts were prepared by lysing attached cells in cold RIPA buffer in the presence of protease inhibitors for HUVECs and HUVSMCs and passive lysis buffer (Promega) for HRMECs. After sonication and centrifugation to remove cell debris, the protein yield was quantified using the BCA protein assay kit (Pierce Biotechnology Inc.). Normalized cell lysates were then mixed with sample buffer containing 2-mercaptoethanol and SDS and heated for 5 minutes at 95°C. Equal amounts of protein were run on SDS-polyacrylamide gels before being transferred to PVDF membranes. Binding of the primary antibodies against p53, p21, and β-actin was detected with enhanced chemiluminescence reagent (Amersham) using HRP-conjugated secondary antibody (1:10,000; Amersham).

Immunofluorescence studies. HUVECs were seeded onto collagen-coated plastic-bottom culture dishes (MatTek Corp.) that were precoated with 0.2% gelatin. Nutlin-3A and Nutlin-3B were diluted to a concentration of 5 μM in X-VIVO medium for 8 hours. Immunofluorescence images with a

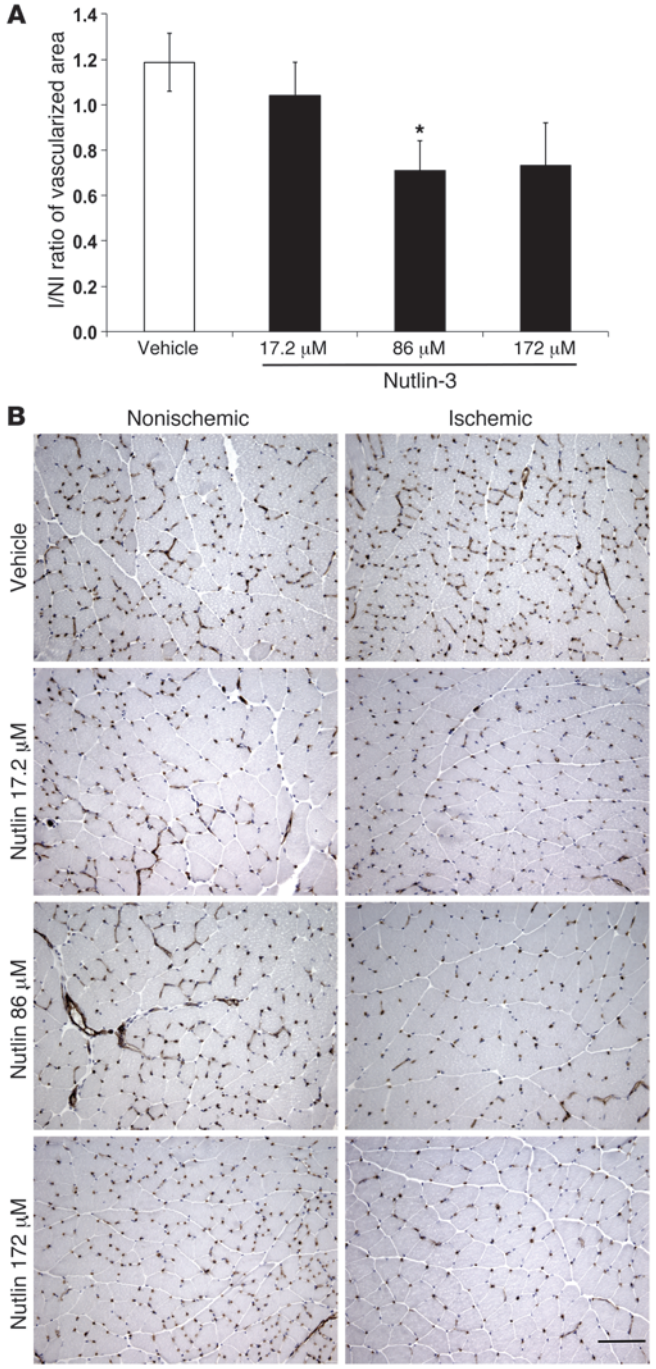

Figure 10
Nutlin-3 inhibited hind limb ischemia–induced neovascularization. (**A**) Quantification of blood capillary density by CD31 immunostaining, expressed as a ratio of ischemic to nonischemic hind limb normalized on myocytes number shows that Nutlin-3 significantly reduced hemangiogenesis when delivered at 86 μM concentration compared with vehicle treatment. At a higher concentration (172 μM), the inhibition was similar but not significant ($n = 5$). (**B**) Representative pictures of CD31 immunostaining of capillaries in nonischemic and ischemic muscles of lower limbs revealed a robust neovascular response at 7 days in the vehicle-treated ischemic hind limb. Treatment with Nutlin-3 resulted in significantly reduced CD31 capillary staining in ischemic hind limb muscles. Data represent mean ± SEM. $^*P < 0.05$. Scale bar: 100 μm.

direct light microscope and fluorescent light were captured using a 3CCD camera and Qcapture imaging software (Qcapture v 2.81; Quantitative Imaging Corp.) or a Carl Zeiss LSM 510 confocal microscope (Carl Zeiss Inc.). For hind limb ischemia, 5 nonserial sections were analyzed for each hind limb. Images were recorded with a digital camera Leica DC480. Densitometric analysis for CD31 and LYVE-1 staining was performed with QwinPro software (Leica). CD31- and LYVE-1–positive areas were normalized to myocyte number and, since CD31 is a panendothelial marker, the blood vessel area was calculated subtracting the LYVE-1–positive area from the CD31-positive area. Ischemic/nonischemic ratio of vascularized area was calculated for each animal.

Flow cytometric analysis for apoptosis. HUVECs and HUVSMCs were incubated with 7.5 μM of Nutlin-3A or DMSO for 24 hours (HUVECs) and 48 hours (HUVSMCs) in X-VIVO medium with FGF-2 (10 ng/ml) and heparin (2 μg/ml). HUVECs were detached with collagenase/EDTA and HUVSMCs were detached with trypsin/EDTA. The cells were then washed twice with PBS and stained with propidium iodide and annexin V–FITC (Annexin V-FITC Apoptosis Detection Kit I, BD) according to the manufacturer's instructions.

TUNEL assay for apoptosis. HUVECs were plated on collagen-coated plastic-bottom culture dishes (MatTek Corp.) overnight. HUVECs were then treated with varying concentrations of Nutlin-3A and Nutlin-3B in X-VIVO medium for 24–72 hours. HRMECs were treated with 15 μM of racemic Nutlin for 24 hours in 10% FBS. The TUNEL assay was performed following instructions provided with the kit (Roche Applied Science). Representative images of the HRMEC experiment were provided with a ×4 objective using an Olympus AX70 fluorescence microscope following the addition of a nuclear counter stain. For HUVEC experiments, 5 representative fields with a ×20 objective using a Zeiss confocal microscope were captured. Two masked observers performed cell counts. For whole-mount retina staining, samples were incubated in TUNEL solution diluted in PBS plus 0.3% Triton-X 100 for 48 hours after lectin staining.

siRNA and shRNA p53 for HUVECs and RRMECs. Passage 3 HUVECs were grown to confluence. shRNA pRETRO-SUPER and pRETRO-SUPER-p53 viruses (gift from Reuven Agami, The Netherlands Cancer Institute, Amsterdam, the Netherlands) were produced by GP2 cells (Clontech) (23). Supernatant was filtered and then added to HUVECs in the presence of 4 mg/ml polybrene followed by 1 μg/ml of Puromycin selection for 7 days. For the RRMEC cell viability assay, RRMECs were seeded at 3000 cells/well in a 96-well plate and allowed to adhere overnight in DMEM supplemented with 10% FBS. The next day, cells were transfected with control siRNA or 2 different siRNA sequences targeting p53 (siRNA p53#1 5′-AGGAUUCACAGUCGGAUdTdT-3′ and siRNA p53#2 5′-CGACAGGGUCACCUAAUdTdT-3′) following lipofectamine protocol (Invitrogen). Twenty-four hours after siRNA transfection, the cells were incubated with 7.5 μM racemic Nutlin-3 or vehicle (DMSO). Cell viability was assessed after 36 hours using CellTiter96 AQueous One Solution Cell Proliferation Assay Kit (Promega) following the manufacturer's instruction.

qRT-PCR for Bax-BCL2. qRT-PCR was performed using an ABI 7500 Fast System (Applied Biosystems) in standard mode. The software used to analyze the data was SDS v. 1.3.1 (Applied Biosystems). qRT-PCR was performed according to ABI standard protocols. The following primer/probe sets were obtained through Applied Biosystems (sense and antisense): β-*actin* (5′-TGACCCAGATCATGTTTGAGA-3′ and 5′-AGTCCATCACGATGCCAGT-3′), *BAX* (5′-AGCTGCAGAGGATGATTGC-3′ and 5′-AGTTGAAGTTGCCGTCAGAA-3′), and *BCL-2* (5′-AGTACCTGAACCGGCACCT-3′ and 5′-CAGCCAGGAGAAATCAAACA-3′). The ΔCt method was used to obtain relative quantification, i.e., Ct values of the target gene

(*BAX*, *BCL-2*) were normalized to the corresponding Ct value of the control gene (β-actin). Relative expression was calculated as follows: relative expression = $(2^{-\Delta Ct}) \times 10{,}000$. No temperature control (NTC) and minus RT controls were run appropriately.

Intravitreal injection for in vivo adult retinal vessel assay. Adult, 3-month-old 129 and C57BL6/129S mice were anesthetized with Avertin and also given a drop of topical proparacaine (1%) for local anesthesia. Using a stereo microscope, a glass capillary pipette was used to inject 1 ml of either vehicle or racemic Nutlin-3 into the vitreous cavity of both eyes of each animal. Mice were then euthanized 5 days after injection.

Preparation of retinal whole mounts. The eyes were then fixed in 4% paraformaldehyde overnight and washed 3 times with PBS. After removing the cornea and lens, the hyaloidal (primitive) vasculature was removed and 4 radial incisions were made in the eyecup to flatten the retina/choroid/sclera complex. The choroid and sclera were removed from the retina and cut at the optic nerve. After the retinal whole mount was blocked with 5% bovine serum albumin, 5% normal donkey serum, and 0.5% Triton X-100 for 3 hours or overnight, the whole mount was incubated with a 1:200 dilution of GS-IB4 lectin overnight and mounted with Vectashield (Vector Laboratories). For double-staining whole-mount experiments, retinas were incubated with primary antibody overnight at 4°C and underwent 6 one-hour washes with PBS-T, followed by incubation with secondary antibody overnight at 4°C, followed by 6 one-hour washes with PBS-T prior to being coverslipped with Vectashield. Using a fluorescent biomicroscope (Carl Zeiss Discovery V12), hyaloidal vessels, vessels connected to the optic nerve, on the surface of the retina, were dissected in a masked manner. A confocal laser (Carl Zeiss LSM 510 meta) was used to obtain images of the retinal vasculature.

Subcutaneous and periocular injection for in vivo retinal development assay. A technique described by Strömblad et al. was modified to study the effects of Nutlin-3 on in vivo vascular development (14). Briefly, racemic Nutlin was administered by subcutaneous injection in the nape or in the periocular area of each eye to WT 129 S1-VIMJ (Jackson Laboratories) mouse pups within 12 hours of birth. The mice received a total of 4 (fused eyelids experiments) or 5 (subcutaneous neck experiments) injections of either racemic Nutlin or 100% DMSO. The first injection of Nutlin was administered at a dose of 40 mg/kg, while the rest were given at a dose of 80 mg/kg for experiments involving injections in the nape. A dose of 80 mg/kg was administered for all injections in the fused eyelid series of experiments. The pups were euthanized on P2 (periocular) or P3 (nape of neck); the eyes were enucleated after the fused eyelids incised.

AAV production. DNAs for the *VMD2*-CRE/GFP constructs were synthesized, inserted into a bacterial plasmid backbone with appropriate AAV1 terminal repeats and a polyadenylation sequence to create AAV1 vector plasmid DNAs, then amplified in *E. coli*. Vector preparations were produced by our standard plasmid cotransfection method (24). Briefly, 1 cell factory containing approximately 10^9 HEK293 cells was transfected by $CaPO_4$ precipitation with a 1:3 molar ratio of AAV vector plasmid DNA and AAV helper plasmid pDG DNA. The cells were harvested 60 hours later, lysed, and the crude lysate purified for vector particles on iodixanol step gradients. Vector-containing fractions were further purified and concentrated by FPLC HiTrap Q Sepharose column chromatography with final concentration and buffer exchanged into Alcon BSS with 0.014% Tween 20. Vector was then titered for DNase-resistant vector genomes by Real-Time PCR relative to a standard vector of known titer. Finally, the purity of the vector was validated by silver-stained SDS–PAGE, assayed for sterility and lack of endotoxin, and then aliquoted and stored at –80°C.

Laser induced CNV model. WT C57BL/6, $p53^{-/-}$, $Hif1a^{flox/flox}$ mice were purchased from Jackson Laboratory. $Vegfa^{flox/flox}$ mice were a gift from Napoleone Ferrara (Genentech). Laser photocoagulation (532 nm, 180 mW, 100 ms, 75 μm) (Ocu-Light GL; IRIDEX Corp.) was performed on both eyes (2–4 spots per eye) of each animal to induce CNV as described (16). 1 μl of racemic Nutlin-3 or 1% DMSO was injected into the vitreous cavity with a 33-gauge microsyringe (Ito Corporation) immediately after laser injury. CNV volumes were measured by scanning laser confocal microscope (TCS SP; Leica) as reported with 0.7% FITC-conjugated GS-IB4 (Vector Laboratories) and quantified using ImageJ Software (NIH) (16). Results are expressed as mean ± SEM (*n* refers to number of laser spots). For subretinal injection experiments, 1 μl of AAV1-*VMD2*-Cre or AAV1-*VMD2*-GFP was injected at 1.0×10^{11} PFU/ml on day 0, with subsequent laser coagulation and Nutlin-3 treatment 6 days later. CNV quantification occurred 7 days after the laser treatment CNV on day 13.

Quantification of retinal vascular development model. We captured images with the same laser power, objective, gain, pinhole, and amplifier offset. The resultant images were masked to the analyst assessing the images. All analyzed images were captured with a ×5 objective and then exported to Adobe Photoshop 7.0 as high-resolution tiff images. Using the Magic Wand tool and histogram function, the analyst recorded the number of pixels that best represented the retinal vasculature and omitted the residual hyaloidal (fetal) vasculature that was unable to be removed during dissection. Blood vessels assessed to be residual hyaloid were found at a different focal plane than retinal blood vessels and were usually connected to the optic nerve.

Hind limb ischemia model. Briefly, C57BL/6J mice ($n = 5$ per group) were anesthetized before unilateral proximal femoral artery ligation (25, 26). The nonischemic left limb underwent a sham surgery without arterial ligation. Immediately following surgery and after 48 hours, Nutlin-3 was intramuscularly administered at 3 different concentrations (17.2, 86, and 172 μM) in a total volume of 30 μl to each hind limb. The same volume of vehicle was injected in ischemic hind limb of control group as well as in the nonischemic left limb of all mice. Seven days later, both anterior and posterior muscles from ischemic and nonischemic hind limbs were harvested, divided into 2 parts by a central transversal cut, and processed for immunohistochemical analysis to quantify angiogenesis and lymphangiogenesis. Sections were prepared starting from the exposed central area versus distal and proximal sides of the muscles.

Statistics. Comparison values were expressed as a percentage or fold difference (means ± SEM). *P* values of less than 0.05 were considered significant and calculated using the Mann-Whitney *U* test (2-tailed), Student's *t* test (2-tailed), or 1-way ANOVA in Microsoft Excel (Microsoft Corp.) or SigmaPlot Ver 12 (Systat Software Inc.).

Study approval. All experiments were performed in accordance with the Weill Medical College of Cornell University and the University of Kentucky Institutional Animal Care and Use Committee. Husbandry of mice for hind limb ischemia procedures was performed in accordance with European Directives no. 86/609 and with Italian D.L. 116. The Institute of Genetics and Biophysics veterinarian approved all the experiments.

Acknowledgments

We would like to acknowledge David Cobrinik for his help with siRNA infection of HUVECs, Sing Your Li for retinal vessel quantification, Loic Vincent for instruction in the Matrigel tube assay, and Dena Almeida for help with immunofluorescence staining. This study was supported in part by grants from the T.J. Martell Foundation for Leukemia, Cancer, and AIDS Research (to T.C. Lee), the Starr Foundation (to T.C. Lee), the Fred Gluck Foundation (to T.C. Lee), the Heed Foundation (to S.H. Chavala), the Charles Kelman Retinal Research Scholar Award (to S.H. Chavala), the International Retinal Research Foundation (to S.H. Chavala), Hope for Vision (to S.H. Chavala), the Research to Prevent Blindness Career Development Award (to S.H. Chavala), a NEI-T32 Vision training

grant (to S.H. Chavala), the Mildred-Scheel-Stiftung (to T. Milde), the Deutsche Krebshilfe, Bonn, Germany (to T. Milde), and Associazione Italiana Ricerca sul Cancro (AIRC) grant IG 11420 (to S. De Falco). J. Ambati was supported by NEI/NIH grants R01EY018836, R01EY020672, R01EY022238, the Doris Duke Distinguished Clinical Scientist Award, the Burroughs Wellcome Fund Clinical Scientist Award in Translational Research, the Ellison Medical Foundation Senior Scholar in Aging Award, a Dr. E. Vernon Smith and Eloise C. Smith Macular Degeneration Endowed Chair, a Research to Prevent Blindness departmental unrestricted grant, and the Carl Marshall Reeves Foundation; N. Kerur was supported by Beckman Initiative for Macular Research Fellowship.

Received for publication October 25, 2012, and accepted in revised form July 11, 2013.

Address correspondence to: Sai H. Chavala, University of North Carolina-Chapel Hill, 5151 Bioinformatics Building, CB7040, Chapel Hill, North Carolina, 27599-7040, USA. Phone: 919.966.5296; Fax: 919.966.1908; E-mail: schavala@med.unc.edu. Or to: Jayakrishna Ambati, Department of Ophthalmology and Visual Sciences, University of Kentucky College of Medicine, 1095 VA Drive, Peter P Bosomworth HSRB, Room 252, Lexington, Kentucky, USA. Phone: 859.257.3902; Fax: 859.257.2317; E-mail: jayakrishna.ambati@uky.edu.

1. Rosenfeld PJ, et al. Ranibizumab for neovascular age-related macular degeneration. *N Engl J Med*. 2006;355(14):1419–1431.
2. Lux A, Llacer H, Heussen FMA, Joussen AM. Non-responders to bevacizumab (Avastin) therapy of choroidal neovascular lesions. *Br J Ophthalmol*. 2007; 91(10):1318–1322.
3. Dugel PU, et al. Macular epiretinal brachytherapy in treated age-related macular degeneration: MERITAGE study: twelve-month safety and efficacy results. *Ophthalmology*. 2012;119(7):1425–1431.
4. Petrarca R, Jackson TL. Radiation therapy for neovascular age-related macular degeneration. *Clin Ophthalmol*. 2011;5:57–63.
5. Canton VM, et al. 24-Gy low-voltage x-ray irradiation with ranibizumab therapy for neovascular AMD: 6-month safety and functional outcomes. *Ophthalmic Surg Lasers Imaging*. 2012;43(1):20–24.
6. Rashi-Elkeles S, et al. Transcriptional modulation induced by ionizing radiation: p53 remains a central player. *Mol Oncol*. 2011;5(4):336–348.
7. Vassilev LT, et al. In vivo activation of the p53 pathway by small-molecule antagonists of MDM2. *Science*. 2004;303(5659):844–848.
8. Secchiero P, et al. Antiangiogenic activity of the MDM2 antagonist Nutlin-3. *Circ Res*. 2007; 100(1):61–69.
9. LaRusch GA, et al. Nutlin3 blocks vascular endothelial growth factor induction by preventing the interaction between hypoxia inducible factor 1alpha and Hdm2. *Cancer Res*. 2007;67(2):450–454.
10. Sermeus A, Michiels C. Reciprocal influence of the p53 and the hypoxic pathways. *Cell Death Dis*. 2011;2:e164.
11. Lee Y-M, et al. Nutlin-3, an Hdm2 antagonist, inhibits tumor adaptation to hypoxia by stimulating the FIH-mediated inactivation of HIF-1alpha. *Carcinogenesis*. 2009;30(10):1768–1775.
12. Patterson DM, et al. Effect of MDM2 and vascular endothelial growth factor inhibition on tumor angiogenesis and metastasis in neuroblastoma. *Angiogenesis*. 2011;14(3):255–266.
13. Song H, Yin D, Liu Z. GDF-15 promotes angiogenesis through modulating p53/HIF-1α signaling pathway in hypoxic human umbilical vein endothelial cells. *Mol Biol Rep*. 2012;39(4):4017–4022.
14. Strömblad S. Loss of p53 compensates for alpha v-integrin function in retinal neovascularization. *J Biol Chem*. 2002;277(16):13371–13374.
15. Park CY, et al. Periocular triamcinolone enhances intraocular gene expression after delivery by adenovirus. *Invest Ophthalmol Vis Sci*. 2008;49(1):399–406.
16. Kleinman ME, et al. Sequence- and target-independent angiogenesis suppression by siRNA via TLR3. *Nature*. 2008;452(7187):591–597.
17. Zhang C, et al. Inhibitory efficacy of hypoxia-inducible factor 1α short hairpin RNA plasmid DNA-loaded poly (D,L-lactide-co-glycolide) nanoparticles on choroidal neovascularization in a laser-induced rat model. *Gene Ther*. 2009;17(3):338–351.
18. Parsons JT, et al. The effects of irradiation on the eye and optic nerve. *Int J Radiat Oncol Biol Phys*. 1983;9(5):609–622.
19. Neovascular Age-Related Macular Degeneration Periocular Corticosteroids Photodynamic Therapy NAPP Trial Research Group, et al. Periocular triamcinolone and photodynamic therapy for subfoveal choroidal neovascularization in age-related macular degeneration. *Ophthalmology*. 2007;114(9):1713–1721.
20. Grossniklaus HE, Kang SJ, Berglin L. Animal models of choroidal and retinal neovascularization. *Prog Retin Eye Res*. 2010;29(6):500–519.
21. Lin M, et al. Impacts of hypoxia-inducible factor-1 knockout in the retinal pigment epithelium on choroidal neovascularization. *Invest Ophthalmol Vis Sci*. 2012;53(10):6197–6206.
22. Zhang F, et al. Whole-body physiologically based pharmacokinetic model for nutlin-3a in mice after intravenous and oral administration. *Drug Metab Dispos*. 2010;39(1):15–21.
23. Brummelkamp TR, Bernards R, Agami R. A system for stable expression of short interfering RNAs in mammalian cells. *Science*. 2002;296(5567):550–553.
24. Hauswirth WW, Lewin AS, Zolotukhin S, Muzyczka N. Production and purification of recombinant adeno-associated virus. *Methods Enzymol*. 2000; 316:743–761.
25. Gigante B, Morlino G, Gentile MT, Persico MG, De Falco S. Plgf$^{-/-}$eNos$^{-/-}$ mice show defective angiogenesis associated with increased oxidative stress in response to tissue ischemia. *FASEB J*. 2006; 20(7):970–972.
26. Cho WG, et al. Small interfering RNA-induced TLR3 activation inhibits blood and lymphatic vessel growth. *Proc Natl Acad Sci U S A*. 2009; 106(17):7137–7142.